Enhancing Transient Stability with Synchronous Condensers under High Offshore Wind Penetration in the New York State Grid

Le Minh Vu
ECE department
Clarkson University
Potsdam, NY, USA
levu@clarkson.edu

Quang-Manh Bui
ECE department
Clarkson University
Potsdam, NY, USA
buimq@clarkson.edu

Jianhua Zhang
ECE department
Clarkson University
Potsdam, NY, USA
jzhang@clarkson.edu

Tony Vu
ECE department
Clarkson University
Potsdam, NY, USA
tvu@clarkson.edu

Thomas H. Ortmeyer
ECE department
Clarkson University
Potsdam, NY, USA
tortmeye@clarkson.edu

***Abstract*—High offshore-wind (OSW) penetration in New York State (NYS) will reduce short-circuit strength and inertia, raising transient-stability concerns. This paper develops an electromagnetic-transient (EMT) reduced model of New York City and Long Island with five aggregated Type-4 OSW plants totaling 5.5 GW under spring light load and summer peak load conditions. Using three-phase point-of-interconnection (POI) faults, critical clearing times (CCTs) are evaluated with and without synchronous condensers (SCs). Results show that appropriately sized SCs installed at the stability-limiting POIs or nearby generator buses can materially increase CCTs by strengthening fault currents, improving voltage recovery, and providing inertia. These findings provide quantitative EMT-level evidence that targeted SC deployment can maintain protection clearing margins as OSW penetration grows.**

***Index Terms*—synchronous condenser (SC), EMT simulation, critical clearing time (CCT), weak grids, offshore wind farms, inverter-based resources (IBRs)**

I. Introduction

The New York State is planning to add significant levels of offshore wind farms (OSWs), including more than 5GW slated for delivery by the early 2030s [1]. At the same time, over 7.2 GW of conventional generation has recently been retired [2], [3]. As these interconnections proceed, increasingly IBR-heavy load pockets will see further erosion of short-circuit strength and inertia as conventional units retire. Recent NYISO assessments and NERC guidance highlight the resulting weak-grid risks and the need to bolster fault current, voltage support, and dynamic VAR reserves as IBR penetration rises [3], [4].

Synchronous condensers (SCs) are a practical near-term ways to harden weak grids. Operated as unloaded synchronous machines, they supply fault current, fast voltage-independent MVAR with short-term field-forcing, and rotational inertia. Large SC programs in South Australia raised export limits and reduced reliance on committed synchronous units, serving as a stability backstop as converter fleets expand [5]. Complementarily, NREL shows pairing SCs with grid-following inverters is an effective interim stabilizing approach while grid-forming deployments scale [6].

For transient stability, a practical metric is the critical clearing time (CCT) defined as the maximum fault duration that can be tolerated without loss of synchronism. It is widely used to set relay clearing times and to quantify the transient-stability margin. In IBR-dominated grids, lower SCR and inertia reduce CCT and narrow protection margins [7]. Large-scale wind integration tends to depress CCT, whereas stronger system strength and added dynamic VAR support increase this metric [8], [9]. In practice, CCT is sensitive to fault location and type, pre-fault dispatch, and controller limits such as PLL bandwidth and current ceilings, which motivates EMT-level assessment. Synchronous condensers extend CCT by supplying fault current that lifts effective SCR, accelerating voltage recovery, and adding rotational inertia [10]. Electromagnetic transient (EMT) studies and field experience also report higher voltage nadirs, faster recovery, reduced commutation-failure risk in AC/DC hybrids, and improved damping of sub- and supersynchronous oscillations when SCs are properly rated [9]–[12]. However, quantified CCT metric for New York City (NYC) and Long Island (LI) with five OSW plants under future load conditions remain limited, where EMT dynamics and urban transmission constraints jointly govern margins.

This paper addresses that gap for NYC and LI grids under high-OSW integration. The main contributions are:

1) Development of EMT reduced models for New York City and Long Island, specific for spring light load and summer peak load cases with five OSW plants totaling 5.5 GW. The reduction preserves fault-level behavior, voltage-recovery dynamics, and converter controls that govern CCT, drawing on weak-grid and HVDC modeling practice.
2) Benchmarking three-phase faults at representative buses and measuring CCT improvements from incremental SC additions relative to the no-SC base.
3) Quantitatively assess how appropriately rated synchronous condensers at weak POIs and synchronous generator buses enhance stability margins to interconnect five OSW plants within protection clearing requirements, and report the associated CCT improvements with explanations of the underlying mechanisms.

979-8-3315-8138-1

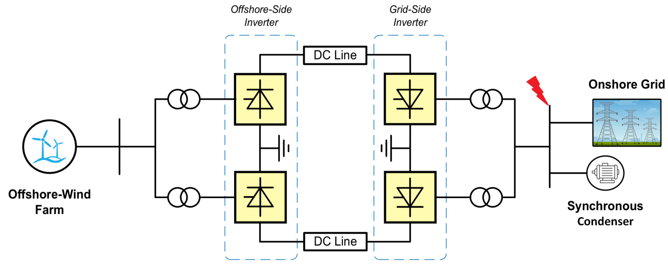

Fig. 1. Configuration of HVDC transmission system connecting OSW farms with onshore grid including a SC connected at POI.

II. System Structure and Working Principle

This section describes the grid topology, offshore-wind plant representations, and synchronous-condenser (SC) modeling framework used to evaluate transient-stability improvements in the New York State grid under high OSW penetration, shown in Fig. 1. The analysis focuses on New York City and Long Island, where multiple large OSW projects are planned to interconnect by 2028 [1].

A. EMT Model of Reduced Onshore NYS Power System

1) Geographic and grid configuration: This research developed a reduced EMT representation of the New York State interconnection focused on NYC and LI. External areas are replaced with dynamic equivalents sized to preserve pre-fault power transfers and short-circuit strength at the study buses. Frequency-dependent, phase-domain line, submarine-cable models and transformer saturation are included to capture realistic fault transients and post-fault recovery. The reduction process is conducted by using E-TRAN Tool [13] with the input data from the Eastern Interconnection MMWG case [14]. The reduced model retains all NYC buses above 345 kV level, all LI buses above 138 kV which is the primary transmission backbones of Zone J and K respectively, and preserves full dynamic models for generators within these areas. Critical OSW POI buses are modeled explicitly, while distant regions are collapsed into coherent dynamic equivalents derived from power-flow data.

2) Operating weak- and strong-grid scenarios: Two 2028 operating points are used: spring light load representing a weak grid and summer peak load representing a strong grid. The weak-grid scenario is characterized by reduced demand and multiple thermal units offline or at minimum generation. This results in lower system inertia and decreased short-circuit capacity, producing a weak grid condition with a lower SCR at key offshore POIs. On the other hand, high demand case keeps more conventional generation online, providing higher inertia and fault current contribution. Consequently, SCR is stronger than weak-grid condition due to in-area generation and network reinforcements, yielding more robust transient stability margins.

B. Offshore Wind Farm and HVDC Modeling

Five OSW farms are integrated into Zone J and K of NYISO, each with capacity between 800–1300 MW. The projects are radially connected at representative 345 kV substations near coastal load centers, capturing realistic network stress at interconnection points.

1) Offshore Wind Farm Modeling: Each OSW farm consists of multiple clusters of aggregated full-converter Type-4 wind turbine generators (WTGs) with hierarchical controls. Machine-side converter (MSC) regulates generator torque via maximum power point tracking (MPPT) with fast current control loops and fault ride-through current limiting, meanwhile grid-side converter (GSC) controls DC-link voltage and reactive power or terminal voltage. Synchronization is achieved by a phase-locked loop (PLL), which is sensitive to POI voltage sags and angle jumps.

Investigating notable size of 5 OSW farms, disturbances from the wind farm systems might cause severe effects on the connected onshore NYS power grid. The plant-level controller is designed to coordinate the response of wind turbine generators during disturbances and ensure stable operating conditions. It has the capability of frequency and voltage support by regulating the total injected active and reactive power into POI.

2) HVDC Transmission System Modeling: Each OSW plant is connected to onshore substation via a half-bridge modular multilevel converter (MMC) bipole. Offshore-side inverter operates in grid-forming mode, controlling the transmission line voltage and wind farm frequency at the offshore collector. On the other hand, grid-side inverter is designed in grid-following mode, regulating DC voltage and supporting AC voltage/reactive power at the POI. For transmission link, a frequency-dependent DC cable model is designed to capture the propagation delays and losses when transmitting the power from offshore to onshore grid.

C. Synchronous Condenser Deployment

1) Placement Rationale: To enhance system strength, one or more SCs are installed at major 345 kV substations near OSW interconnection points in Zones J and K, with the objectives to increase short-circuit MVA at weak buses, provide dynamic reactive power for voltage recovery, and contribute rotational inertia to slow down frequency and angle excursions.

2) Modeling Framework: Each SC is represented as a round-rotor synchronous machine operating without a prime mover and exchanging no real power.

Electrical machine: Subtransient dynamics on the d– and

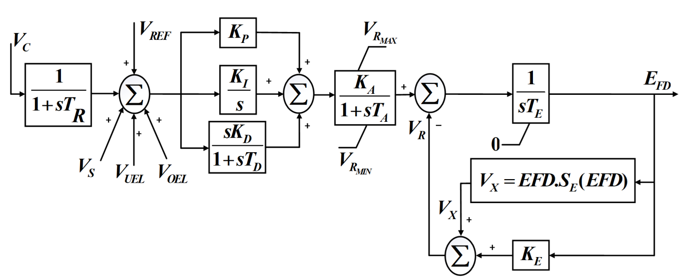

Fig. 2. Synchronous condenser AC exciter model (AC8B, Basler DECS-type).

q–axes (X_d'', X_q'' with associated time constants and damper windings) are retained to capture the large first-cycle fault current and its subsequent decay.

Excitation/Automatic Voltage Regulator (AVR): The regulator follows the IEEE AC8B (Basler DECS-type) structure as defined in IEEE Std 421.5-2016 [15]. As shown in Fig. 2, the measured terminal voltage is filtered by a transducer (T_R) and compared with a reference together with supervisory inputs (e.g., stabilizer V_S, underexcitation limiters (UEL), and overexcitation limiters (OEL)) to form the control error. A proportional–integral–derivative (PID) controller with lead–lag compensation drives the AVR amplifier (K_A, T_A) and the exciter/field block (T_E). Static feedback and the open-circuit saturation characteristic $S_E(\cdot)$ produce realistic ceiling behavior and short-term field forcing. The UEL and OEL limiters protect the field while permitting brief over-excitation for dynamic MVAR support. In steady state the AVR regulates $V_C \approx V_{\text{ref}}$ in Fig. 2. During faults, it supplies fast, largely voltage-independent reactive current up to the modeled limits.

Mechanical system: Governed by the swing equation:

$$2H\frac{d\omega}{dt} = T_m - T_e - D(\omega - \omega_s), \qquad T_m \approx 0,$$

where H is the inertia constant in seconds, defined as the stored kinetic energy at rated speed divided by the machine MVA base; T_m and T_e are the mechanical input and electromagnetic air-gap torques in per unit on the torque base, and for a synchronous condenser $T_m \approx 0$; ω is the rotor speed in per unit of the synchronous speed ω_s; and D is the damping coefficient expressed as per-unit torque per unit speed deviation. The stored kinetic energy is $E_k = H\,S_{\text{base}}$, and this inertia resists frequency deviations.

All excitation-system parameters (gains, time constants, and limiters) are selected within IEEE Std 421.5-2016 recommended ranges [15]. Machine-side parameters (subtransient/transient reactances and time constants, damper data) are taken from planning-grade manufacturer data/templates and tuned to meet voltage-response and short-term ceiling targets, ensuring credible fault-level support in EMT simulations.

D. Working Principle of SCs in Transient Stability

SCs enhance stability through three primary mechanisms. Firstly, high subtransient currents support POI voltage during faults, reducing converter saturation, and stabilizing PLL synchronization in the first few cycles of electromagnetic response. For over hundreds of milliseconds excitation response, AVR-driven reactive-power injection accelerates post-fault voltage recovery and increases synchronizing torque. Finally, rotational inertia slows frequency and angle divergence, extending CCT and damping post-fault oscillations in case of over-seconds inertia response.

In addition, SC also coordinates with OSW converters and HVDC controls to secure stability margins. The dynamic VAR support from SC complements the converter-limited VAR capability in OSW plants whereas AVR droop is coordinated with MMC Q/V control to prevent control conflicts. By boosting short-circuit strength and fault voltage recovery, SCs enable OSW converters remain stable during disturbances.

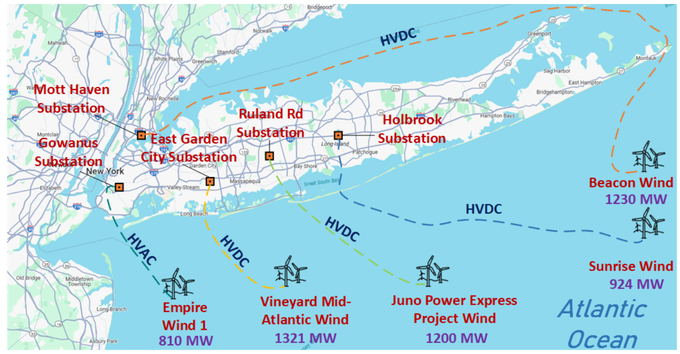

Fig. 3. Strategic NYS OSW Deployment: Substations, Wind Farms, Atlantic-Ocean Interconnection

III. Case Studies

A. Studied System and Operating Scenarios

This research studies the EMT reduced models of NYC and LI transmission areas with five aggregated Type-4 OSW farms. The total 5.5 GW rating power of five OSW farms is injected at different POIs with two substations in NYC and three ones in LI. Offshore wind project capacities and transmission technologies are illustrated in Fig. 3 with four HVDC systems and one HVAC link. Unless otherwise stated, all OSWs are dispatched at 100% nameplate rating in this study. All studies are initialized from a solved AC power flow, and the EMT integration step is $\Delta t = 10\ \mu$s.

Two specific operating scenarios are evaluated including spring 2028 light load and summer 2028 peak load. The comparison between base case and SC-installed case is implemented in both scenarios. SCs are installed at the buses that set the CCT limit in the baseline, i.e., the locations where instability first emerges: the OSW POI exhibiting PLL/ride-through loss and the unstable generator bus showing initial rotor-angle divergence.

B. Disturbances and CCT Evaluation

A bolted three-phase-to-ground fault is applied at the onshore substation of the targeted OSW POI, as shown in Fig. 1, which represents the worst case for CCT assessment. The fault clearing time is varied in small increments until the CCT is identified, while the offshore wind plant remains electrically connected through its transmission system. Pre-fault dispatch, fault location, and protection logic are held identical across both "with and without SC" cases for each seasonal scenario.

Transient stability performance is then evaluated using four metrics: (i) CCT, defined as the maximum fault duration t_f that still yields post-fault re-stabilization; (ii) voltage nadir and recovery, which is the minimum POI (or nearby bulk-bus) voltage and the time to recover to 0.90 p.u. of voltage level; (iii) converter performance, including PLL tracking and OSW low-voltage ride-through capability; and (iv) rotor-angle boundedness for synchronous devices. A case study is deemed

979-8-3315-8138-1

stable if voltages recover, converters remain connected and re-ramp, and no growing angle divergence is observed. Otherwise it is unstable (e.g., increasing angle separation or sustained voltage depression).

C. Baseline Stability without Synchronous Condensers

This subsection presents EMT results for a bolted three-phase-to-ground fault at the OSW POIs and establishes the baseline CCTs without SCs.

Scenario 1 (spring 2028, light load): With all five OSW plants online, a bolted three-phase fault is applied at a POI in LI. The baseline CCT is 5 cycles at 60 Hz, approximately ≈ 83.3 ms. The first component to lose stability under three-phase fault event is the HVDC-export OSW connected at a weak POI, indicating that converter dynamics combined with limited LI grid strength set the stability limit. As shown in Fig. 4, the HVDC demonstrated the low-voltage ride through capability with a 5-cycle three-phase fault. The POI voltage dips to about 0.25 p.u., overshoots to about 1.18 p.u., and returns near nominal within 1 s. When clearing is delayed to 6 cycles, recovery fails and the post-fault voltage rings around 0.5–0.6 p.u., the HVDC PLL loses tracking and does not promptly re-lock. The current controller remains at its limit, and DC link oscillations grow, confirming converter instability.

Scenario 2 (summer 2028, peak load): With all five OSW plants online, a bolted three-phase-to-ground fault is applied at a POI in NYC. The baseline CCT is 8 cycles. In the three-phase-fault case, the first units to lose synchronism are the nearby natural-gas generators at a POI close to the fault. This indicates that the stability limit is set by local synchronous inertia and the units' electrical proximity to the disturbance. When the clearing time is delayed to 9 cycles, the affected units exhibit sustained rotor-angle divergence and trip once protection thresholds are exceeded. Fig. 5 shows rotor-angle trajectories in radians, and some synchronous generator units' rotor angle diverges, indicating the system instability.

D. Stability With Synchronous Condensers

This subsection quantifies the CCT increase when SCs are installed at the buses that set the baseline limit—the weak OSW POI in spring and the generator step-up (GSU) transformer high-side bus in summer. The same fault setup and pass/fail criteria as the baseline are used.

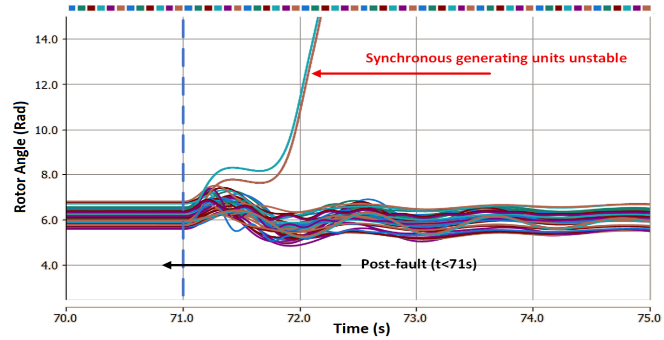

Fig. 5. Rotor-angle trajectories (rad) of synchronous gas units for 9-cycle clearing of a three-phase POI fault (summer 2028, no SC).

Scenario 1 (spring 2028, light load + SC at OSW POI): With a 250 MVAR SC connected at the weak LI POI, the system exhibits a higher stability margin under three-phase fault. The baseline CCT increases from 5 cycles to 17 cycles. Under 18 cycles, the first component to lose stability remains the HVDC-export OSW at the same weak POI. For the 17–cycle case, the HVDC onshore terminal inverter rides through with shorter current–limit dwell and maintains PLL locked. As shown in Fig. 6, the POI voltage dips to around 0.20 p.u., then overshoots to under 1.20 p.u., and returns to steady-state condition within under 1.5 s. By contrast, the 18–cycle case fails to recover to flat start condition. Fig. 6 compares the 17– vs. 18–cycle terminal–voltage traces, showing sustained low–voltage ringing around 0.5–0.6 p.u. and ensuing converter instability at 18 cycles. Compared to the no–SC baseline in Fig. 4, the system in this case tolerates over three times longer under three-phase fault events before re–stabilizing.

Scenario 2 (summer 2028, peak load + SCs at GSU high–side bus): SCs are installed at the unstable GSU high-side bus. With one 250 MVAr SC, the CCT for the three-phase POI fault increases from 8 to 11 cycles, as shown in Fig. 7. At 12 cycles the nearby gas units exhibit sustained rotor-angle divergence and trip once protection thresholds are exceeded. Adding two 250 MVAr units for a total of 500 MVAr at the

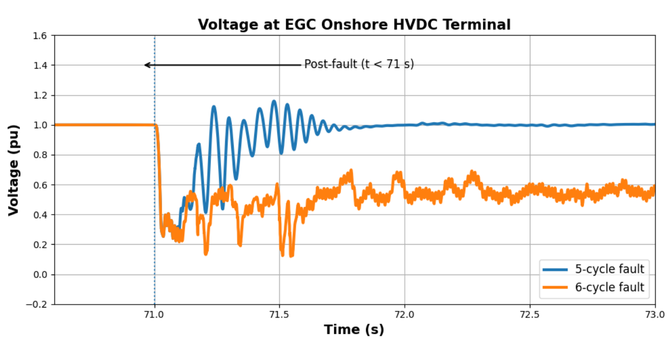

Fig. 4. HVDC terminal voltage at the OSW POI for 5- and 6-cycle clearing of a three-phase POI fault (spring 2028, no SC).

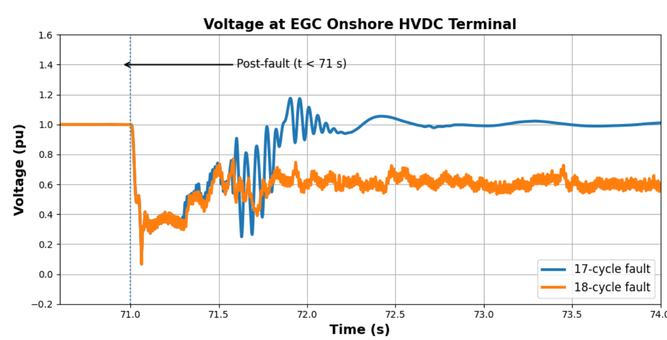

Fig. 6. HVDC terminal voltage at the OSW POI for 17– and 18–cycle clearing of a three–phase POI fault (spring 2028, with 250 MVAR SC).

979-8-3315-8138-1

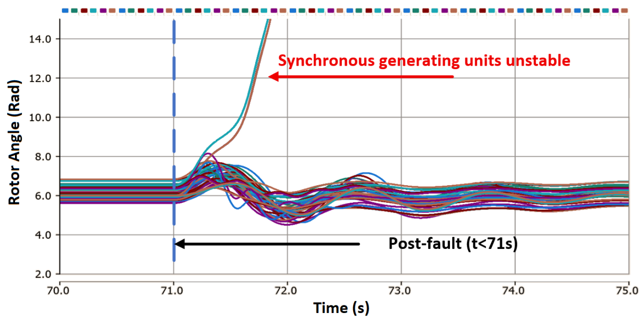

Fig. 7. Rotor-angle trajectories (rad) of nearby synchronous gas units for 12-cycle clearing of a 3-phase POI fault (summer 2028, one 250 MVAR SC).

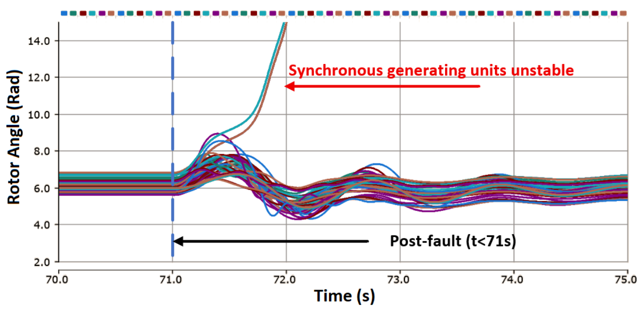

Fig. 8. Rotor-angle trajectories (rad) of nearby synchronous gas units for 14-cycle clearing of a 3-phase POI fault (summer 2028, two 250 MVAR SCs).

same bus extends the CCT to 13 cycles, as shown in Fig. 8, while instability reappears at 14 cycles.

E. Summary and Discussion

Across both operating scenarios, SCs deliver quantified CCT enhancements. In spring 2028 light load, adding a 250 MVAR SC at the weak Long Island POI raises the CCT from 5 to 17 cycles, and the HVDC-export OSW at that POI becomes unstable at 18 cycles. In summer 2028 peak load, installing one 250 MVAR SC at the unstable GSU high-side bus increases the CCT from 8 to 11 cycles, with instability at 12 cycles. With two 250 MVAR units at the same bus, the CCT rises to 13 cycles, and instability appears at 14 cycles.

These improvements arise from three complementary mechanisms of SCs. Firstly, stronger fault-current support stiffens the network during the fault, raising effective SCR at the study bus and shortening converter current-limit dwell while helping the PLL maintain locked. Secondly, fast excitation from the AC8B regulator supplies short-term MVAR that lifts the voltage nadir and reduces the time–voltage sag area, so voltages recover sooner after clearing faults. Thirdly, synchronous inertia tempers speed and angle excursions, delaying loss of synchronism of nearby machines. When the converter ride-through at a weak POI is the binding constraint, siting a SC at that POI provides the largest benefit. When the CCT limit is synchronous angle stability near the fault, a SC at the generator bus is more effective. SC sizing assessment shows that the first 250 MVAR provides the largest step increase, while doubling to 500 MVAR yields smaller but meaningful additional margin and can increase short-circuit duty.

IV. Conclusion

This study proved that adding SCs at targeted locations materially enlarges transient-stability margins for NYC and LI under a high–offshore-wind scenario by conducting EMT-based CCT assessment. In both seasonal scenarios, SCs increased short-circuit strength and voltage support, shifting the stability limit to longer permissible clearing times for three-phase POI fault events. Future work will co-optimize SC sizing and placement with relay clearing times and short-circuit constraints, test sensitivity to converter controls, compare against non-rotating compensators, and extend the framework to multi-contingency studies and cost-benefit analyses.

Acknowledgment

The authors gratefully acknowledge the National Offshore Wind Research and Development Consortium (NOWRDC Award 192899-132) for supporting this research, “Atlantic Seaboard Offshore Stability Risk Evaluation & Service.” The authors also thank our GE Vernova partners (Jason MacDowell, Neethu Abraham), NYPA AGILe (Thanh Nguyen), and the project’s Industry Advisory Board for their perspectives.

References

[1] New York State Energy Research and Development Authority, “About offshore wind.” [Online]. Available: https://www.nyserda.ny.gov/All-Programs/Offshore-Wind/About-Offshore-Wind
[2] L. Kearney, “Ny power grid faces shortfalls as new energy supply lags, operator says,” Reuters, Jun. 2024.
[3] New York Independent System Operator, “Power trends 2024.” [Online]. Available: https://www.nyiso.com/documents/20142/2223020/2024-Power-Trends.pdf
[4] North American Electric Reliability Corporation (NERC), “Integrating inverter-based resources into low short circuit strength systems,” 2017.
[5] Australian Energy Market Operator (AEMO), “Operation of davenport and robertstown synchronous condensers.”
[6] R. W. Kenyon, A. Hoke, J. Tan, and B.-M. Hodge, “Grid-Following Inverters and Synchronous Condensers: A Grid-Forming Pair?” in *2020 Clemson University Power Systems Conference*. IEEE, Mar. 2020.
[7] P. Moore, O. A. Alimi, and A. Abu-Siada, “A Review of System Strength and Inertia in Renewable-Energy-Dominated Grids: Challenges, Sustainability, and Solutions,” *Challenges*, no. 1, p. 12, Feb. 2025.
[8] Y.-K. Wu, T.-C. Lee, T.-Y. Hsieh, and W.-M. Lin, “Impact on critical clearing time after integrating large-scale wind power into Taiwan power system,” *Sustainable Energy Technologies and Assessments*, Aug. 2016.
[9] L. Bao, L. Fan, and Z. Miao, “Wind farms in weak grids stability enhancement: SynCon or STATCOM?” *Electric Power Systems Research*, vol. 202, p. 107623, Jan. 2022.
[10] X. Luo, F. Li, L. Fan, T. Niu, B. Li, L. Tian, and H. Yu, “Influence of Synchronous Condensers on Operation Characteristics of Double-Infeed LCC-HVDCs,” *Processes*, vol. 9, no. 10, p. 1704, Sep. 2021.
[11] S. Teleke, T. Abdulahovic, T. Thiringer, and J. Svensson, “Dynamic Performance Comparison of Synchronous Condenser and SVC,” *IEEE Transactions on Power Delivery*, no. 3, pp. 1606–1612, Jul. 2008.
[12] P. Ying, Z. Qidi, L. Xuan, H. Yiping, and X. Guorui, “Influence of Synchronous Condenser on Voltage Stability of HVDC,” in *2018 IEEE PESGM*. Portland, OR: IEEE, Aug. 2018, pp. 1–5.
[13] E. Corporation, “E-tran software,” 2025. [Online]. Available: https://electranix.com/software/
[14] “ERAG eastern interconnection – MMWG reliability assessment,” https://www.rfirst.org/eastern-interconnection-reliability-assessment-group/, ReliabilityFirst.
[15] *IEEE Recommended Practice for Excitation System Models for Power System Stability Studies*, IEEE Power & Energy Society Std. IEEE Std 421.5-2016, 2016, revision of IEEE Std 421.5-2005.